Lifting-Surface Theory for Propfan Vortices Impinging on a Downstream Wing

R. Martinez*
Cambridge Acoustical Associates, Inc., Cambridge, Massachusetts

Retrofitment of commercial aircraft with propfans could introduce undesirable aerodynamic sources of structure-borne noise that are absent for current turbojet powerplants. This paper theoretically examines the whipping action of the vortex wake from a generic propeller on the downstream rigid wing that supports it. The model addresses the high-frequency/compressible regime of most anticipated propfan implementations and produces an analytic solution for the distributed wing airload due to the periodic vortex impingement. The analysis also yields an expression for the local unsteady lift obtained from integration over an arbitrary internal patch of wing surface, for the purpose of applying a practical number of such forces at the nodes of a finite-element model for the corresponding structure (wing response results are not included in the present paper). Reported estimates of induced wing loads for a conventional-propeller example of demonstration appear to be in the reasonable range of expectation.

Nomenclature

b = wing half-chord, dimensional normalizing constant
b_j = jth chordwise point, nondimensional
c_0 = sound speed, dimensional
E^* = Fresnel integral
h_0 = instantaneous normal-to-wing vortex position, $\tilde{R}\sin(\Omega t+\phi_n)$, Fig. 1
k = $\omega b/U$, reduced frequency
L_{mN} = harmonic of piecewise airload, dimensional (force)
M = flight Mach number
m = harmonic number
N = number of blades
p_{mN} = wing pressure distribution for harmonic counter m, dimensional
R = propeller radius normalized by b
$\tilde{R}$ = Rb, propeller radius
s_j = jth spanwise point, nondimensional
T = total propeller thrust
T_0 = blade-passage period $2\pi/(\Omega N)$, dimensional
t = time, dimensional, Fig. 1
U = flight speed, dimensional
w = total propeller-induced downwash velocity, dimensional
$w_{mN}, \tilde{w}_{mN}$ = time Fourier component of w, dimensional, and its normalized spanwise Fourier transform, Eq. (9)
w_v = contribution of a single vortex to the total downwash function, Fig. 1
x = normal-to-leading-edge coordinate, nondimensional;
y = spanwise coordinate, nondimensional
$\tilde{y}$ = yb
$\tilde{y}_0$ = instantaneous position of vortex along span, $\tilde{R}\cos(\Omega t+\phi_n)$, Fig. 1
β = $\sqrt{1-M^2}$
θ = blade pitch of representative radial station
Γ = vortex strength, dimensional
μ = wave-number parameter, kM/β^2
$\tilde{\mu}$ = $\sqrt{\mu^2-(\lambda/\beta)^2}$, Eq. (7)
ϕ_n = $2\pi(n-1)/N$, phase factor for blade n, Fig. 1
ρ = background density, dimensional
Ω = propeller rotational speed, rad/s
ω = $m\Omega N$

Introduction

THIS communication summarizes the fluid-model part of a study of structural vibrations induced by the vortex wake of a propeller.[1,2] Our theoretical treatment revisits the old blade-vortex interaction problem of numerous investigations that sought to understand it experimentally or analytically (e.g., Ahmadi,[3] and Martinez and Widnall[4]), but with the reciprocal twist that now an aircraft's stationary wing replaces the familiar rotorblade, and the single vortex becomes a turning system of potential vortices, one for each propeller blade tip. The present development considers the high-frequency and high flight-speed regime of the phenomenon and thereby complements Weir's analysis for incompressible flow.[5]

The aerodynamic model conceived in Ref. 6 predicted the continuous unsteady airload distribution over a rigid wing of infinite span in the vortex wake of a tractor propeller [Eq. (7)]. The propeller wake was composed of a system of infinite and straight potential vortices in rotary motion (Fig. 1) and was assumed to be unaffected by the presence of the wing. At each

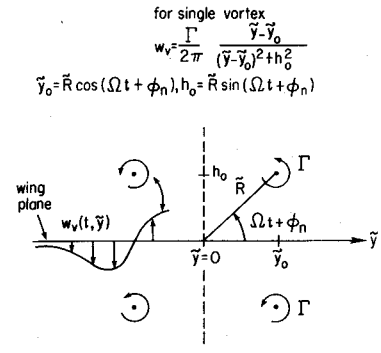

Fig. 1 Wake model for a four-bladed propeller indicating horizontal plane of wing and downwash induced by upper-left vortex.

Presented in part as Paper 87-2681 at the AIAA 11th Aeroacoustics Conference, Palo Alto, CA, Oct. 19-21, 1987; received April 2, 1988; revision received Dec. 6, 1988.

*Senior Scientist. Member AIAA.

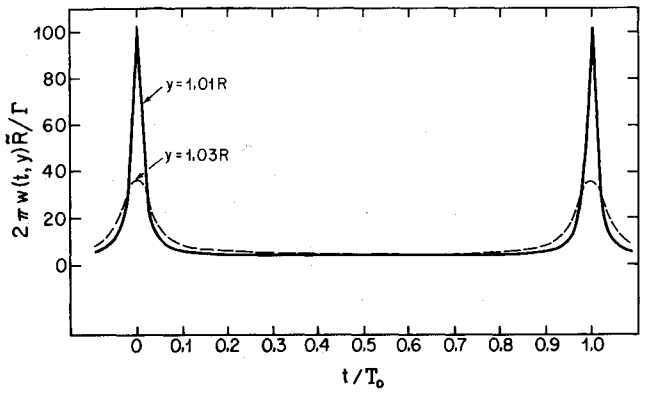

Fig. 2 History of normalized downwash for wake model, $w(t=0,y)\to\infty$ as $y\to R$.

spanwise station the resulting downwash function was constant over the chord and therefore constituted a simplified version of that found by Hardin for vortex filaments of finite curvature[7]; its numerical evaluation was confined to a surface region corresponding to an unswept wing of infinite span with parallel leading and trailing edges. Calculation of the unsteady pressure distribution followed upon Fourier transformation of the boundary-value problem in the spanwise variable, application of Amiet's lift/downwash transfer function for a plunging airfoil at high frequency and flight speed[8] (since the imposed downwash was constant over the chord), and upon final return transformation to physical spanwise space.

This paper extends the aerodynamic calculation of Ref. 6 by deriving an analytic expression for the concentrated point lift resulting from a local closed-form integration of the existing pressure function, with a view to later applying such an airload at a chosen node of the finite-element model of the wing structure.[9] The theoretical result of unsteady piecewise lift over an arbitrary interior segment of chord represents a generalization of Amiet's formula for the whole airfoil.

Development

Analytical Features of Modeled Downwash Distribution

Figure 2 shows the normalized time signature of the expression for the modeled downwash in Fig. 1 [Eqs. (1) and (2)] at two sample span stations just outside the chord line of intersection for each blade-tip vortex and the wing surface; the time origin has been chosen to be the vortex/wing cutting instant at $y/R=1$. We complete Ref. 6 by drawing some physical interpretations of the downwash solution:

$$w(t,y)=\sum_{n=1}^{N} w_v(t,y;n) \tag{1}$$

re-expressed there as

$$w(t,y)=\frac{\Gamma N}{2\pi\tilde{R}}\begin{cases}\sum_{m=0}^{\infty}\cos(mN\Omega t)f_1(y,m) & \text{for} \quad |y|>R \quad (2a)\\ -\sum_{m=1}^{\infty}\cos(mN\Omega t)f_2(y,m) & \text{for} \quad |y|<R \quad (2b)\end{cases}$$

where $f_1(y,m), f_2(y,m)$ are, respectively, defined for $|y|>R$, $|y|<R$:

$$f_1(y,m)=(R/y)^{Nm+1} \qquad |y|>R \tag{3a}$$

$$f_2(y,m)=(y/R)^{Nm-1} \qquad |y|<R \tag{3b}$$

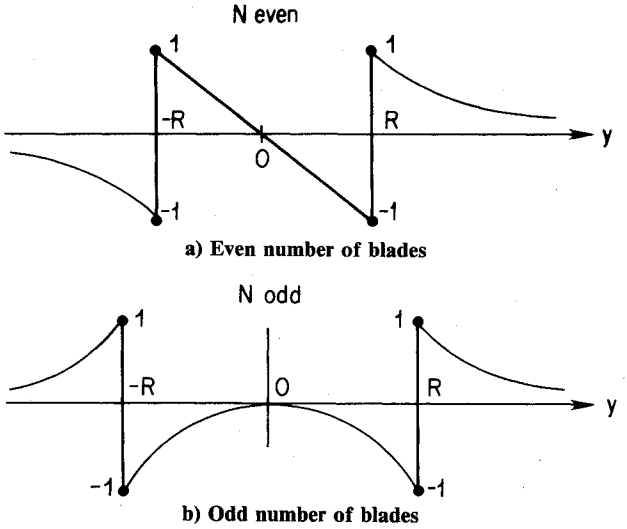

Fig. 3 Spanwise behavior of normalized downwash fundamental, $4\pi\tilde{R}w_N/\Gamma N$, for a propeller with

Reference 6 has cast Eqs. (2a) and (2b) in terms of exponential harmonics

$$w(t,y)=\frac{\Gamma N}{4\pi\tilde{R}}\sum_{m=-\infty}^{\infty} e^{imN\Omega t}\begin{cases}\nu_m f_1(y,|m|) & (4a)\\ (\delta_{om}-1)f_2(y,|m|) & (4b)\end{cases}$$

where $\nu_{m=0}=2$, $\nu_{m>0}=1$; $\delta_{0m}=1$ for $m=0$ and zero otherwise. With

$$w(t,y)=\sum_{m=-\infty}^{\infty} e^{imN\Omega t}w_{mN}(y) \tag{5}$$

it follows that w_{mN} is given by the product of $\Gamma N/(4\pi\tilde{R})$ and the functions within brackets in Eqs. (4a) and (4b).

The sum in Eq. (2a) starts with $m=0$ whereas that in Eq. (2b) starts with $m=1$. It is of incidental interest that Eq. (3a) yields $f_1(y,m=0)=R/y$ and thus implies that the rotating vortices in Fig. 1 collectively induce a downwash pattern that has a nonzero steady component over wing stations outside the propeller diameter, i.e., over $|y|>R$. Function f_1 is odd in y for $m=0$, and its associated steady angle-of-attack distribution along the span should generate a likewise steady aerodynamic moment about the propeller axis. It is interesting also to note that Eqs. (2a), (2b), and (3b) are consistent with the intuitively static situation that comes about from letting $N\to\infty$; Eq. (2b) then collapses to zero [since $y/R<1$ in Eq. (3b)], and Eq. (2a) is left with only the $m=0$ term. These limits are in turn consistent with the behavior of the analogous electrostatics problem for which the field inside the cylindrical-shell conductor is zero, whereas that outside it may be interpreted as caused by a single charge at the center.[10]

Of primary relevance to the wing vibration/cabin noise problem is the $m=1$ term of $w(t,y)$, i.e., its blade passage, or fundamental component $w_N(y)$ from Eq. (5) (since higher components are negligible by comparison in their contribution to total noise). Equations (3a) and (3b) lead to the conclusion that $w_N(y)$ is odd in y when the number of blades N is even, and even in y when N is odd (Fig. 3). Reference 6 has shown that the associated airload distribution is obtained from the convolution of $FT[w_N(y)]\propto\bar{w}_N(\lambda)$ and an aerodynamic transfer function that is even in transform wave number λ (see Eq. III.24, p. 30 of Ref. 6), resulting in a loading solution that agrees spatially with the odd/even character of its driving downwash, i.e., airloads are even in y when N is odd and odd in y when N is even. Reference 6 addressed a case for which the number of blades N was even (8), and so generated predictions of wing pressures that were odd in y and thus zero at the

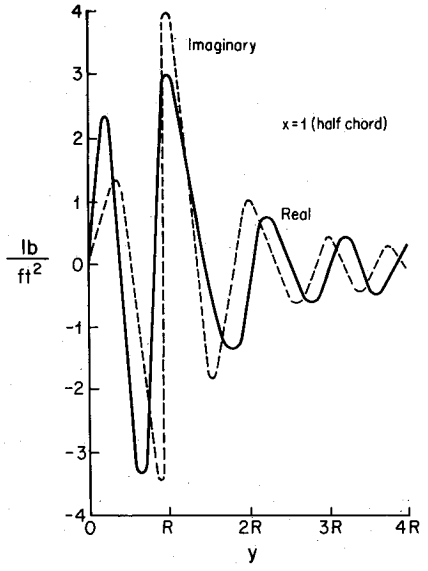

Fig. 4 Predicted spanwise pressure distribution along midchord line $x = 1$ (from Ref. 6). Signal displays the acoustic wavelength for points far from $y = 0$.

propeller axis station $y = 0$ (see Fig. 4, which is Fig. III.9 of Ref. 6 and shows the pressure distribution in the spanwise direction for the midchord line for the half-range $y > 0$ of a wing surface). Here we shall demonstrate the new lifting-surface theory for a smaller aircraft with a propeller having $N = 3$. The calculated loading will therefore be even about and generally nonzero at the propeller axis station $y = 0$.

Figure 5 explains graphically why an odd number of blades produces a downwash function $w(t,y)$ with a blade-passage component $w_N(y)$ that is even in y (without loss of generality the example uses $N = 3$). The sketch shows that

$$w(t_0 + T_0/2, y>0) = -w(t_0, y<0)$$

where t_0 is an arbitrary value of time, and T_0 is blade-passage period $2\pi/\Omega N$. Equations (2a) and (2b) have proved that the temporal periodicity of $w(t,y)$ is strictly in terms of cosines, so that by definition $w_N(y>0)$ can be obtained from

$$w_N(y>0) = \frac{1}{T_0}\int_0^{T_0} dt\; w(t,y>0)\cos\left(\frac{2\pi t}{T_0}\right) \tag{6a}$$

[although this was not an a priori assumption in Ref. 6 to arrive at Eqs. (2a) and (2b)]. In view of the above pictorial argument, the definition of $w_N(y<0)$ is

$$\begin{aligned} w_N(y<0) &= -\frac{1}{T_0}\int_0^{T_0} dt w\left(t+\frac{T_0}{2},\, y>0\right),\, y>0)\cos\left(\frac{2\pi t}{T_0}\right) \\ &= -\frac{1}{T_0}\int_{T_0/2}^{3T_0/2} dt w(t,y>0)\cos\left[2\pi\left(\frac{t-T_0}{2}\right)/T_0\right] \\ &= \frac{1}{T_0}\int_{T_0/2}^{3T_0/2} dt w(t,y>0)\cos\left(\frac{2\pi t}{T_0}\right) \\ &= \frac{1}{T_0}\int_0^{T_0} dt\; w(t,y>0)\cos\left(\frac{2\pi t}{T_0}\right) \\ &= w_N(y>0) \end{aligned} \tag{6b}$$

One may simply show that

$$w_N(y>0) = -w_N(y<0)$$

whenever N is even, as depicted in the upper part of Fig. 3.

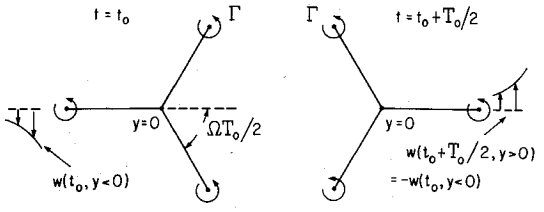

Fig. 5 Positions of vortices for instants t_0 and $t_0 + T_0/2$ for a case with three blades.

Lifting-Surface Theory for Airloads Induced by Trailing Vortices from a Tractor Propeller at High Flight Speed

The distributed airload on the wing's lower surface has been found to be (see Ref. 6, Eq. III.26)

$$\begin{aligned} p_{mN}(x,y,0^-) &= \frac{\rho U\Gamma N}{\beta\bar{R}}\frac{(1+i)}{2\pi^2} \\ &\times \int_0^\infty \frac{d\lambda}{\sqrt{\tilde{\mu}^2-\mu^2M^2}}\left\{kE^*[(\tilde{\mu}-\mu M)x] - i\sqrt{\frac{\tilde{\mu}-\mu M}{2\pi x}}\right. \\ &\times \exp[-i(\tilde{\mu}-\mu M)x] + E^*[(\tilde{\mu}+\mu M)(2-x)] - \left.\left(\frac{1-i}{2}\right)\right\} \\ &\times Re\left\{\exp\left(\frac{i\pi}{2}(N\mid m\mid +1) - i\lambda y\right)\tilde{w}_{mN}(\lambda)\right\} \end{aligned} \tag{7}$$

with Re denoting real part and

$$E^*(a) \equiv \int_0^a \frac{dt e^{-it}}{\sqrt{2\pi t}} \tag{8}$$

$$\begin{aligned} \tilde{w}_{mN} &= \frac{\nu_m R^{N\mid m\mid +1}}{(N\mid m\mid)!} \\ &\times \left\{\sum_{j=1}^{N\mid m\mid}\lambda^{j-1}\frac{(N\mid m\mid -j)!\cos[\lambda R - \frac{\pi}{2}(N\mid m\mid -j+2)]}{R^{N\mid m\mid -j+1}}\right. \\ &\left. -\frac{\lambda}{\mid\lambda\mid}\,si(\mid\lambda\mid R)\cdot\lambda^{N\mid m\mid}\right\} + \frac{(1-\delta_{mo})(N\mid m\mid -1)!}{R^{N\mid m\mid -1}} \\ &\times \left\{\sum_{j=1}^{N\mid m\mid -1}\frac{R^{N\mid m\mid -j}(-1)^{j+1}}{\lambda^j(N\mid m\mid -j)!}\cos[\lambda R - \frac{\pi}{2}(N\mid m\mid +j-1)]\right. \\ &\left. + \frac{\sin\lambda R}{\lambda^{N\mid m\mid}}\right\} \end{aligned} \tag{9}$$

where again $\nu_m = 2,1$ for $m = 0, \neq 0$, respectively; $\delta_{mo} = 1$ for $m = 0$ and 0 otherwise; si is the sine integral

$$si(z) = -\int_z^\infty dt\,\frac{\sin t}{t} \tag{10}$$

From Eq. (7) we now seek the net lift concentrated at a typical control point $(b_j + b_{j+1})/2$, $(s_j + s_{j+1})/2$,

$$\begin{aligned} &L_{mN}\left(\frac{b_j+b_{j+1}}{2}, \frac{s_j+s_{j+1}}{2}\right) \\ &\equiv 2b^2\int_{s_j}^{s_{j+1}} dy\int_{b_j}^{b_{j+1}} dx\; p_{mN}(x,y,0^-) \end{aligned} \tag{11}$$

where all spatial variables within and including the integral signs have been normalized by wing semichord b. The factor of 2 appearing on the right side reflects the inherent wing-plane load antisymmetry of the lifting flow.

Figure 6 displays a typical subrectangle centered at normalized position

$$(b_j + b_{j+1})/2,\ (s_j + s_{j+1})/2$$

For simplicity of notation we shall now set j equal to 1 with the understanding that in the resulting expressions b_2 can play the role of any b_{j+1} and b_1 that of any b_j. The same rule will apply in the interpretation of s_1 and s_2. Interchanging orders of integration, the chordwise calculation results in the quadrature over segment $b_1 < x < b_2$ of the quantity within in Eq. (7). Each of the four contributing terms may be evaluated in closed form, e.g.,

$$\int_{b_1}^{b_2} dx\, E^*[(\tilde{\mu} + \mu M)(2-x)$$

$$= \left[b_2 - 2\left(1 + \frac{\frac{i}{4}}{\tilde{\mu} + \mu M}\right)\right] E^*[(\tilde{\mu} + \mu M)(2-b_2)]$$

$$- \left[b_1 - 2\left(1 + \frac{\frac{i}{4}}{\tilde{\mu} + \mu M}\right)\right] E^*[(\tilde{\mu} + \mu M)(2-b_1)]$$

$$+ \frac{i}{\sqrt{2\pi(\tilde{\mu} + \mu M)}} \left\{\sqrt{2-b_2}\, \exp[-i(\tilde{\mu} + \mu M)(2-b_2)]\right.$$

$$\left. - \sqrt{2-b_1}\, \exp[-i(\tilde{\mu} + \mu M)(2-b_1)]\right\} \qquad (12)$$

Equation (12) is easily obtained through integration by parts with "dv" = dx. The final result for a general chordwise segment is

$$\int_{b_1}^{b_2} dx \left\{kE^*[(\tilde{\mu} + \mu M)x] - i\sqrt{\frac{\tilde{\mu} - \mu M}{2\pi x}}\, e^{-i(\tilde{\mu} - \mu M)x}\right.$$

$$\left. + E^*[(\tilde{\mu} + \mu M)(2-x)] - \left(\frac{1-i}{2}\right)\right\} = \left(\frac{1-i}{2}\right)(b_1 - b_2)$$

$$+ \left[kb_2 + \frac{ik/2}{\tilde{\mu} - \mu M} - i\right] E^*[(\tilde{\mu} - \mu M)b_2]$$

$$- \left[kb_1 + \frac{ik/2}{\tilde{\mu} - \mu M} - i\right] E^*[(\tilde{\mu} - \mu M)b_1] + \frac{i/k}{\sqrt{2\pi(\tilde{\mu} - \mu M)}}$$

$$\times \left\{\sqrt{b_1}\, e^{-i(\tilde{\mu} - \mu M)b_1} - \sqrt{b_2}\, e^{-i(\tilde{\mu} - \mu M)b_2}\right\}$$

$$+ \left\{b_2 + 2\left[1 + \frac{i/4}{\tilde{\mu} + \mu M}\right]\right\} E^*[(\tilde{\mu} + \mu M)(2-b_2)]$$

$$- \left\{b_1 - 2\left[1 + \frac{i/4}{\tilde{\mu} + \mu M}\right]\right\} E^*[(\tilde{\mu} + \mu M)(2-b_1)]$$

$$+ \frac{i}{\sqrt{2\pi(\tilde{\mu} + \mu M)}} \cdot \left\{\sqrt{2-b_2}\, \exp[-i(\tilde{\mu} + \mu M)(2-b_2)]\right.$$

$$\left. - \sqrt{2-b_1}\, \exp[-i(\tilde{\mu} + \mu M)(2-b_1)]\right\} \qquad (13)$$

Similarly, integration over spanwise segment $s_1 < y < s_2$ relies on the following simple identity:

$$\int_{s_1}^{s_2} dy e^{-i\lambda y} = i/\lambda\, (e^{-i\lambda s_2} - e^{-i\lambda s_1}) \qquad (14)$$

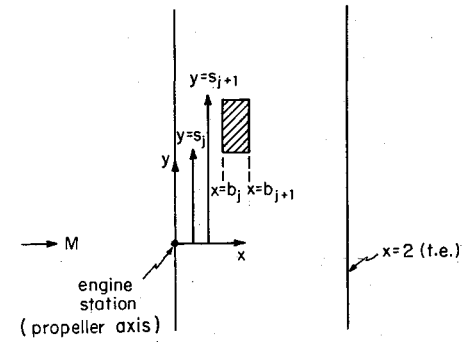

Fig. 6 Schematic of wing surface showing elemental rectangle over which the pressure distribution has been integrated to yield a concentrated force.

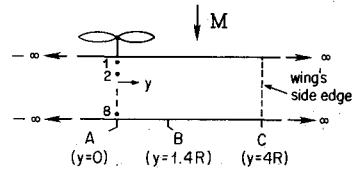

Fig. 7 Plan view of wing surface indicating positions of three sample stations.

Table 1 Commuter-class aircraft cruise operating parameters[11]

Cruise thrust/engine lb	338
Cruise speed, ft/s	407
Cruise altitude, ft	22,000 ft ($c_0 \cong 1024$ ft/s, $M \approx 0.4$)
Number of blades N	3 } = BFF = 135 Hz
Engine rpm, Hz	45
Propeller radius $\tilde{R}$, in.	39
Wing chord $2b$ at engine station, in	58

Table 2 Predicted point airloads (lb) for wing stations A, B, C of Fig. 7

Chord point	A: $y = 0$		B: $y \cong 1.4R$		C: $y = 4R$	
	$Re(L_N)$	$Im(L_N)$	$Re(L_N)$	$Im(L_N)$	$Re(L_N)$	$Im(L_N)$
1	0.458	0.257	0.573	0.142	0.125	−0.0345
2	−0.198	0.294	0.404	0.477	0.145	0.0381
3	−0.346	0.298	0.453	0.562	0.185	0.0550
4	−0.460	0.276	0.518	0.604	0.221	0.0638
5	−0.541	0.244	0.573	0.633	0.248	0.0708
6	−0.589	0.216	0.603	0.648	0.260	0.0760
7	−0.607	0.201	0.604	0.641	0.254	0.0757
8	−0.589	0.205	0.573	0.580	0.230	0.0621

Airload Prediction for a Typical Business-Class Aircraft

Table 1 lists cruise operating parameters for a medium-sized commercial aircraft. They justify application of our high-speed, high-frequency, unsteady aerodynamic model by yielding a value for $\mu = kM/\beta^2 = \Omega N b/(c_0\beta^2)$ of about 2.4, corresponding to a tonal fundamental $\Omega N/2\pi$ of 135 Hz.[11]

Table 2 shows predictions for three wing stations, marked A, B, and C, respectively, at the propeller axis $y = 0$, at $y = 1.4R$ (where load magnitudes turn out to be maximum), and at $y = 4R$ (Fig. 7); $S_{j+1} - S_j = R/5$ for all j. The tabulated unsteady forces display chordwise maxima for the real part near the midchord spanwise line and nonzero levels along the trailing edge. The latter effect is an artifact of the aerodynamic theory, which is based on an iterative procedure for flows about the leading and trailing edges in a sequence of correction steps (see explanations in Refs. 6 and 8; another

obvious deficiency is the prediction of nonzero lift at the station corresponding to the tip side edge, at $y = 4R$, for the actual aircraft's wing). As earlier stated, airloads for the $y = 0$ chord are not zero because the number of blades for the example is odd, rather than even as in Fig. 4. The values displayed are samples from a detailed tabulation carried out in Ref. 12; their integration over the indicated outboard extent of wing surface results in $26 + i6$ lb of total unsteady lift, or 8% of the design engine thrust that produces it (338 lb).

The author is not aware of experiments in the compressible speed range against which his theory could be tested. Any such future attempts at comparison for an aircraft roughly fulfilling the reduced frequency/Mach number criterion of this example should begin by properly scaling up (or down) the results in Table 2 according to the difference in value of the overall multiplicative force constant

$$\rho U T N(2b^2)/\tilde{R}$$

between the present case and the new situation [Eqs. (7) and (11)]. The vortex strength Γ used in the calculations was the result of applying in a simple roll-up model the lifting-line relationship for maximum blade sectional "lift" $L_{\max}$ for the 75% radial station

$$\rho\Gamma\sqrt{U^2 + (0.75\Omega\tilde{R})^2} = L_{\max} \tag{15}$$

and of assuming a triangular distribution between blade hub and tip to give the total blade thrust T/N; θ denotes pitch angle for the blade radial station of maximum running thrust:

$$\frac{1}{2}L_{\max}(0.75\tilde{R}) = \frac{T}{N}\sec\theta \tag{16}$$

The numbers so obtained should be halved if they are to be compared to measurements that record the unsteady pressure on only one surface of the wing, i.e., half the local lift assuming the loading is antisymmetric about the wing plane. Also, it should be remembered that the theory here lumps the pressure distribution acting over a small rectangular patch segment of wing into a single force at its center, so that each such control point contains a "basin" around it and the basins add up to the total wing surface area. If measurements are conducted with a set of wing-mounted sensors in such a way that the force felt by each reflects only the local value and, thus, excludes pressures acting over surrounding intersensor basin surfaces, the scaling process obviously would also have to take proper account of differences in sensor/sensor-basin areas.

Conclusions

We have developed a lifting-surface theory for wing airloads caused by a system of potential vortices trailing from a tractor propeller; its regime of validity is the moderate-to-high subsonic Mach number range and high reduced frequency based on blade rate. Our analysis generalized the calculation of lift presented in Ref. 8 to apply to an arbitrary internal chord segment rather than to the entire wing cross section, because its ultimate aim is to use such piecewise-discrete forces in a structural model that requires them at a fairly textured set of chosen nodal points. Reported sample airload predictions for a typical commuter aircraft appear to be in the physically reasonable range of expectation.

Acknowledgments

The work was conducted for NASA Langley Research Center under NASA Grant NAS1-18020. The author wishes to thank his colleague, Ann Westagard Stokes, for her help with the computation.

References

[1]Cole, J. E., Westagard Stokes, A., Garrelick, J. M., and Martini, K., "Analytical Modeling of the Structure-borne Noise Path on a Small Twin-Engine Aircraft," NASA CR-4136, June 1988.

[2]Cole, J. E. and Martini, K., "Structure-borne Noise Measurements on a Small Twin-Engine Aircraft," NASA CR-4137, June 1988.

[3]Ahmadi, A. R., "An Experimental Investigation of the Chopping of Helicopter Main Rotor Tip Vortices by the Tail Rotor," NASA CR-177338, Sept. 1984.

[4]Martinez, R. and Widnall, S. E., "An Aeroacoustic Model for High-Speed, Unsteady Blade-Vortex Interaction," *AIAA Journal,* Vol. 21, Sept. 1983, pp. 1225–1231.

[5]Weir, D. S., "Wing Loads Induced by a Propeller Wake," AIAA Paper 86-1976, 1986.

[6]Martinez, R., "Predictions of Unsteady Wing and Pylon Forces Caused by Propeller Installation," NASA CR-178298, May 1987.

[7]Hardin, J. C., "The Velocity Field Induced by a Helical Vortex Filament," *Physics of Fluids,* Vol. 25, Nov. 1982, pp. 1949–1952.

[8]Amiet, R. K., "High-Frequency Thin-Airfoil Theory for Subsonic Flow," *AIAA Journal,* Vol. 14, Aug. 1976, pp. 1076–1082.

[9]Martinez, R., Cole, J. E., Martini, K., and Westagard, A., "All-Theoretical Prediction of Cabin Noise due to Impingement of Propeller Vortices on a Wing Structure," AIAA Paper 87-2681, Oct. 1987.

[10]Morse, P. M. and Feshbach, H., *Methods of Mathematical Physics,* McGraw-Hill, New York, 1953, p. 217.

[11]"Performance Parameters of U.S. Business, Personal, Utility Aircraft," *Aviation Week & Space Technology,* March 1986, p. 158.

[12]Martinez, R., "Calculation of Point Forces over a Wing for Tractor Propeller Tip-Vortex Excitation," Cambridge Aeronautical Associates CAA TM/U-1465-349.17, Feb. 1987.